

Supplementary Material of “On the Approximation of the Entire Pareto Front of a Constrained Multi-objective Optimization Problem”

Angel E. Rodriguez-Fernandez^{1[0000-0002-2157-8077]}, Carlos Hernández^{2[0000-0003-4303-6866]}, and Oliver Schütze^{1[0000-0003-4970-9574]}

¹ Computer Science Department, Cinvestav, Mexico

{angel.rodriguez@,schuetze@cs.}cinvestav.mx

² IIMAS-UNAM, Mexico

carlos.hernandez@iimas.unam.mx

1 The EqCo Benchmark

This benchmark consists of five bi-objective functions (EqCo1-5) with 2,3 and 5 decision variables. They are designed to visualize the behaviour of the CHTs on problems of increasing difficulty. EqCo1 ($n = 2$) has the simple constraint $x_2 = 0$, meaning that the PS is a the line joining (-1,0) and (1,0). The constraints of EqCo2, EqCo3 and EqCo4 ($n = 3, 2, 3$) imply that feasible points have to be on the unit sphere (or the unit circle for EqCo3). The PS for EqCo2 is an arc on the unitary sphere, for EqCo3 it is an arc on the unit circle, and for EqCo4 is a complex geodesic on the unit sphere. EqCo5 ($n = 5$) was taken from [1], where the PS is a complex curve. An additional problem, *emptyps*, was designed to have an empty PS.

1. EqCo1

$$\begin{aligned} F : [-1.5, 1.5]^2 &\rightarrow \mathbb{R}^2 \\ F(x) &= (f_1(x), f_2(x))^\top \\ f_i(x) &= \|x - a^i\|^2 \\ s.t. \\ h(x) &= x_2 \\ \text{with:} \\ a^1 &= (-1, -1), \quad a^2 = (1, 1) \end{aligned}$$

2. EqCo2

$$\begin{aligned}
F : [-2, 2]^3 &\rightarrow \mathbb{R}^2 \\
F(x) &= (f_1(x), f_2(x))^\top \\
f_1(x) &= (x_1 - a_1^1)^4 + (x_2 - a_2^1)^2 + (x_3 - a_3^1)^2 \\
f_2(x) &= (x_1 - a_1^2)^2 + (x_2 - a_2^2)^4 + (x_3 - a_3^2)^2 \\
&\text{s.t.} \\
h(x) &= \|x - c\| - r
\end{aligned}$$

with:

$$a^1 = (1, 1, 1), \quad a^2 = (1, 1, -1), \quad c = (0, 0, 0), \quad r = 1$$

3. EqCo3

$$\begin{aligned}
F : [-11, 11]^2 &\rightarrow \mathbb{R}^2 \\
F(x) &= (f_1(x), f_2(x))^\top \\
f_1(x) &= (x_1 - a_1^1)^2 + (x_2 - a_2^1)^2 \\
f_2(x) &= (x_1 - a_1^2)^2 + (x_2 - a_2^2)^2 \\
&\text{s.t.} \\
h(x) &= \|x - c\| - r
\end{aligned}$$

with:

$$a^1 = (0, -10), \quad a^2 = (10, 0), \quad c = (0, 0, 0), \quad r = 1$$

4. EqCo4

$$\begin{aligned}
F : [-1.5, 1.5]^3 &\rightarrow \mathbb{R}^2 \\
F(x) &= (f_1(x), f_2(x))^\top \\
f_1(x) &= (x_1 - a_1^1)^4 + (x_2 - a_2^1)^2 + (x_3 - a_3^1)^2 \\
f_2(x) &= (x_1 - a_1^2)^2 + (x_2 - a_2^2)^4 + (x_3 - a_3^2)^2 \\
&\text{s.t.} \\
h(x) &= \|x - c\| - r
\end{aligned}$$

with:

$$a^1 = (0.8, 0, 0), \quad a^2 = (0, 0.5, 0.5), \quad c = (0, 0, 0), \quad r = 1$$

5. EqCo5

$$\begin{aligned}
F &: [-2, 2]^5 \rightarrow \mathbb{R}^2 \\
F(x) &= (f_1(x), f_2(x))^\top \\
f_1(x) &= \|x\|^2 \\
f_2(x) &= 3x_1 + 2x_2 - \frac{x_3}{3} + 0.01(x_4 - x_5)^3 \\
s.t. \\
h_1(x) &= x_1 + 2x_2 - x_3 - 0.5x_4 + x_5 - 2 \\
h_2(x) &= 4x_1 - 2x_2 + 0.8x_3 + 0.6x_4 + 0.5x_5^2
\end{aligned}$$

6. emptyps

$$\begin{aligned}
F &: [-3, 3]^2 \rightarrow \mathbb{R}^2 \\
F(x) &= (f_1(x), f_2(x))^\top \\
f_i(x) &= \|x - a^i\|^2 \\
s.t. \\
h_1(x) &= \|x - a^1\|^2 - r^2 \\
h_2(x) &= \|x - a^2\|^2 - r^2 \\
\text{with:} \\
a^1 &= (-2, 0), \quad a^2 = (2, 0), \quad r = 1
\end{aligned}$$

2 Effect of μ on the CPF approach.

Additional tests were performed to manually determine the value of μ for each problem. Specifically, five runs were conducted for each problem using μ values of 1, 2, 5, 8, and 10. For the EqCo benchmark, a random sampling method was used, with a population size of 100 and 1,000,000 function evaluations for all problems, except for EqCo1 and EqCo3, where 100,000 and 10,000 function evaluations were used, respectively. For the Eq1DTLZ benchmark, a population size of 100 and 100,000 function evaluations were applied.

Our experiments revealed three distinct behaviors: (a) μ has minimal effect, (b) smaller values of μ lead to infeasible points, whereas larger values of μ yield feasible solutions, and (c) higher values of μ result in a ‘cleaner’ solution. Figures 2, 3, and 7 illustrate examples for cases (a), (b), and (c), respectively.

The values selected for the experiments are: $\mu = 1$ for EqCo1 and EqCo2, $\mu = 2$ for EqCo4 and EqCo5 and Eq1DTLZ1-4, $\mu = 5$ for Eq1IDTLZ1, and $\mu = 10$ for EqCo3 and Eq1IDTLZ2.

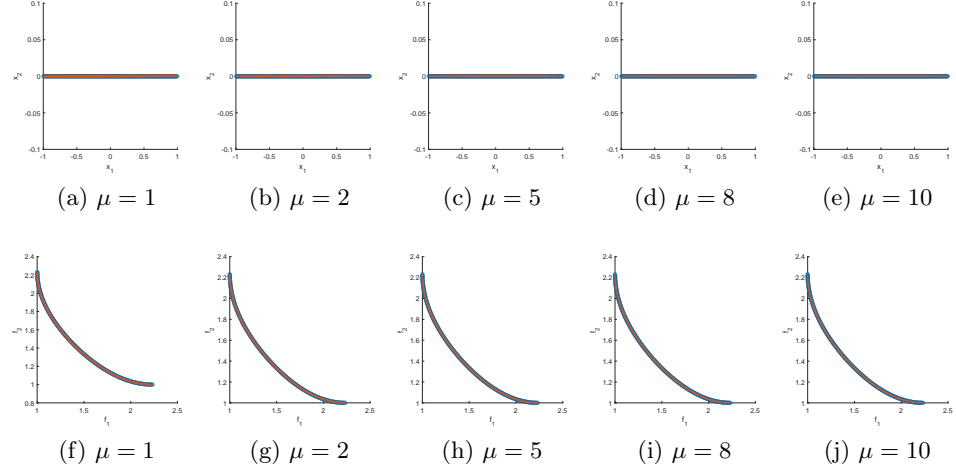


Fig. 1. Effect of μ for the problem EqCo1.

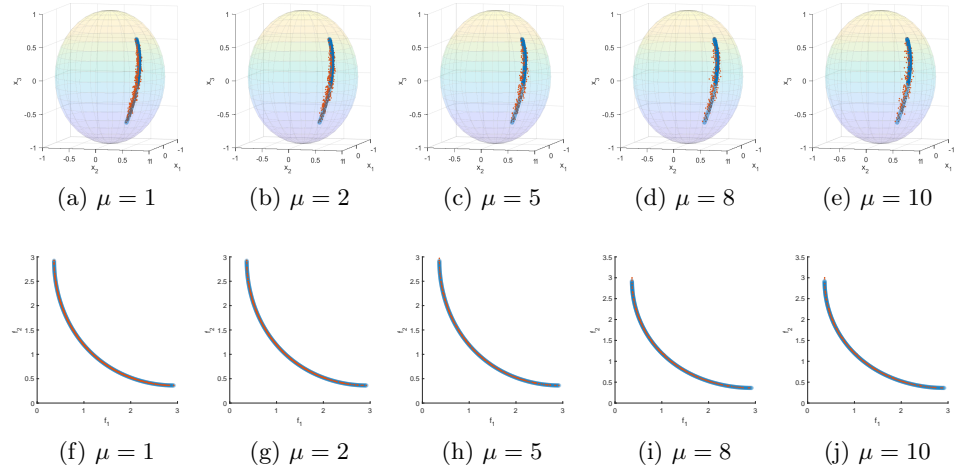
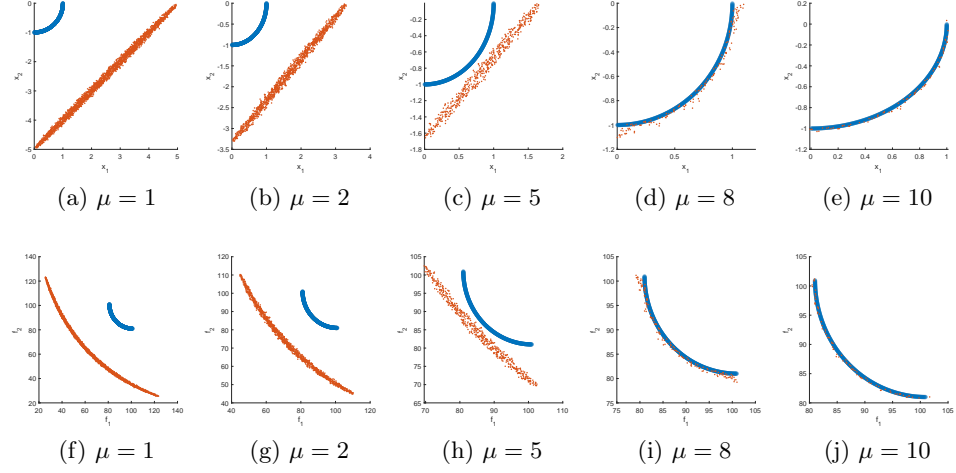
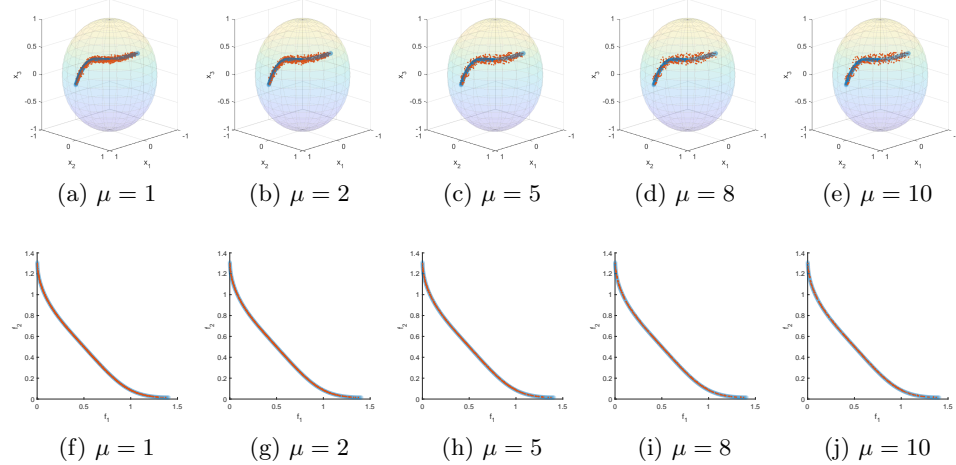
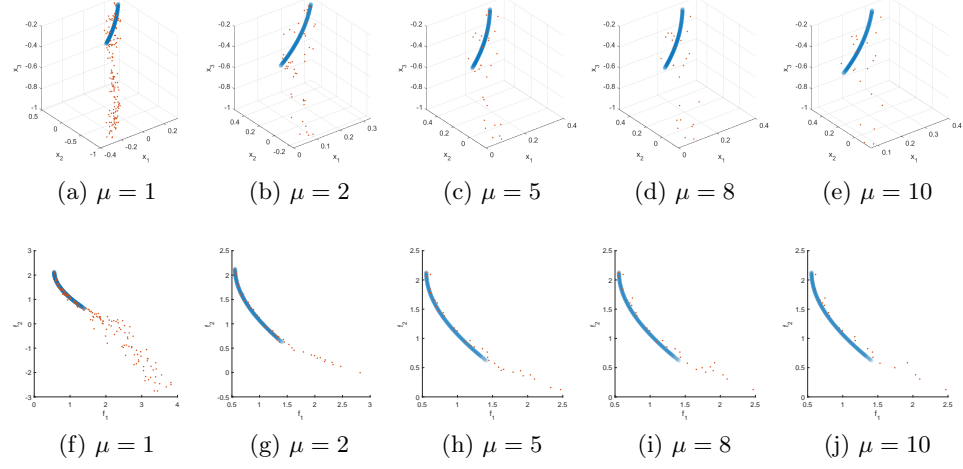
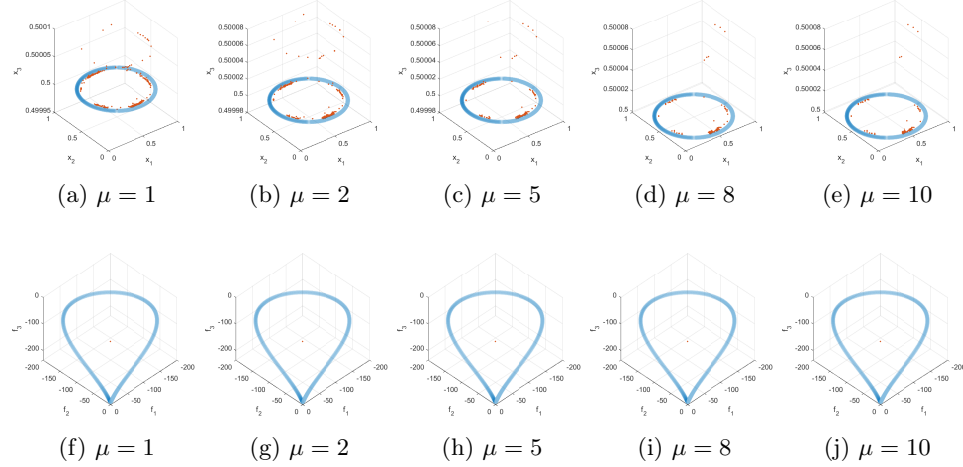
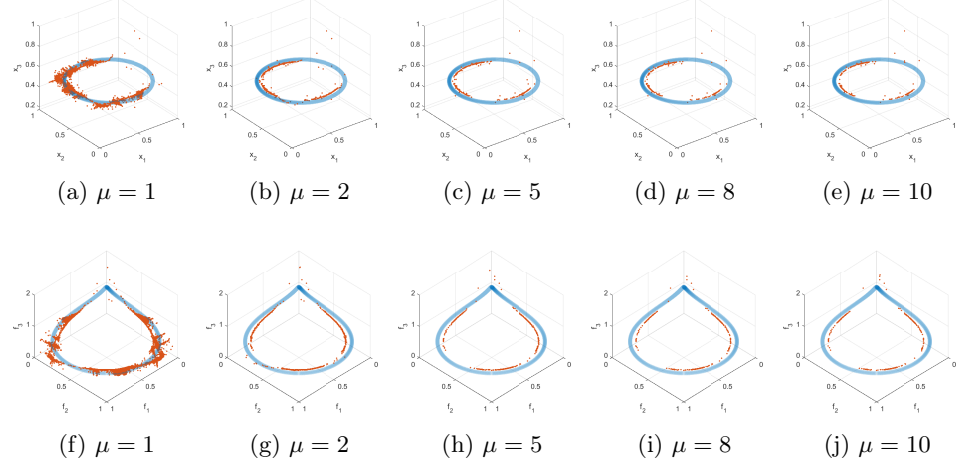
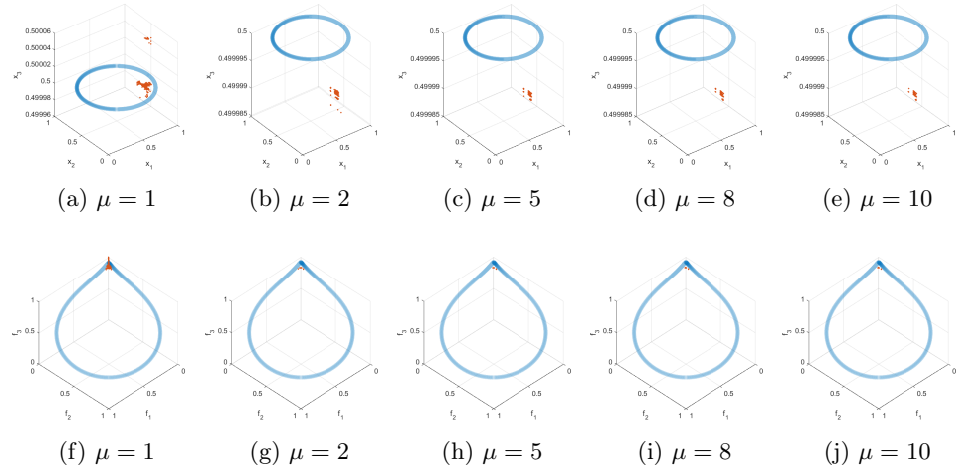
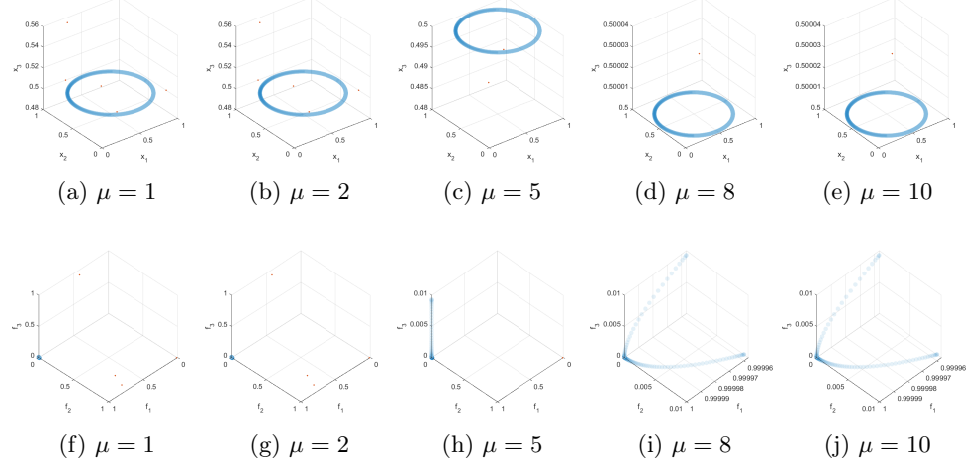
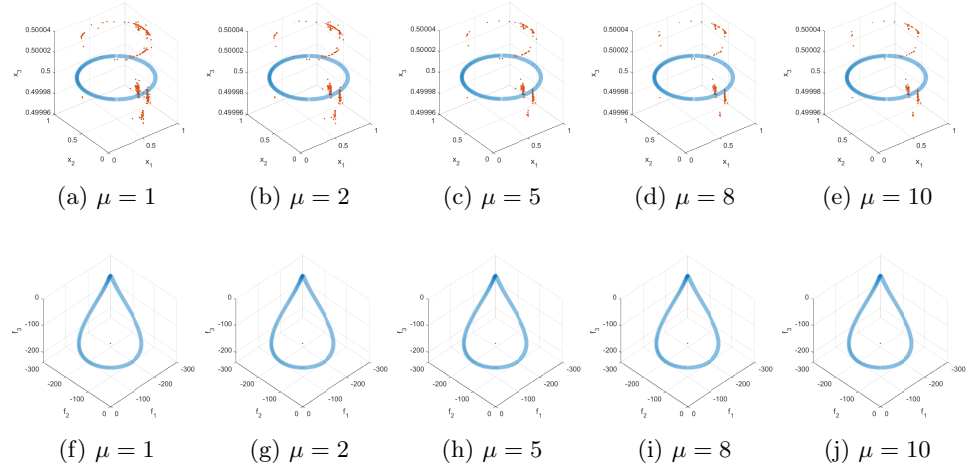


Fig. 2. Effect of μ for the problem EqCo2.

**Fig. 3.** Effect of μ for the problem EqCo3.**Fig. 4.** Effect of μ for the problem EqCo4.

**Fig. 5.** Effect of μ for the problem EqCo5.**Fig. 6.** Effect of μ for the problem Eq1_DTLZ1.

**Fig. 7.** Effect of μ for the problem Eq1_DTLZ2.**Fig. 8.** Effect of μ for the problem Eq1_DTLZ3.

**Fig. 9.** Effect of μ for the problem Eq1_DTLZ4.**Fig. 10.** Effect of μ for the problem Eq1_IDTLZ1.

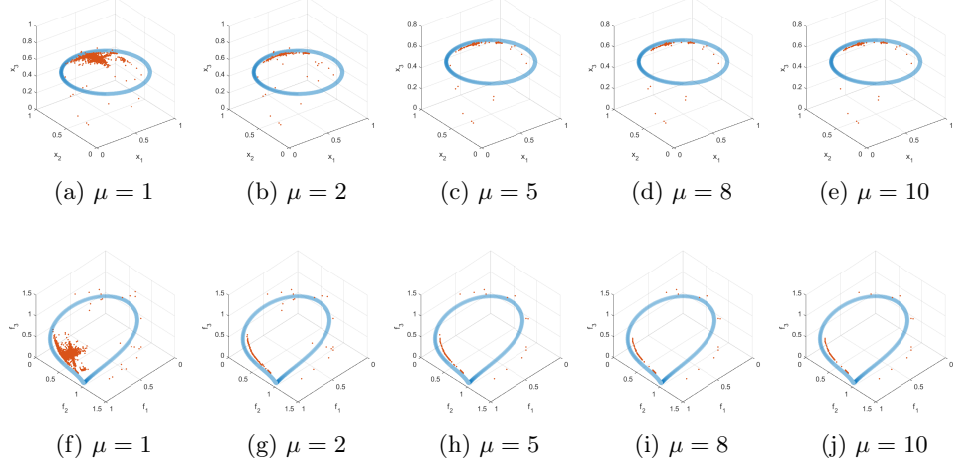


Fig. 11. Effect of μ for the problem Eq1_IDTLZ2.

3 Experimental Results

In the following figures (Figures 12–22), we present the result plots from the first run for all problems, MOEAs, and archivers, as described in the main manuscript.

We observe that, in general, using an external archiver produces better solutions than the standalone MOEA. However, there are some exceptions, such as the CDP approach with C-TAEA for the EqCo2 problem (Figure 13). Surprisingly, for this problem (EqCo2), NSGA-II is the MOEA that finds the best solutions among all methods.

Another interesting result is shown in Figure 12, where, despite all the MOEAs ignoring the constraints, all the archiving approaches still manage to find a better approximation of the PF.

Finally, we observe difficulties with the MOEAs in finding feasible solutions across all problems, particularly in the Eq1DTLZ benchmark. In general, if the MOEA struggles to find feasible solutions, we cannot expect the archive to provide a good approximation of the PF.

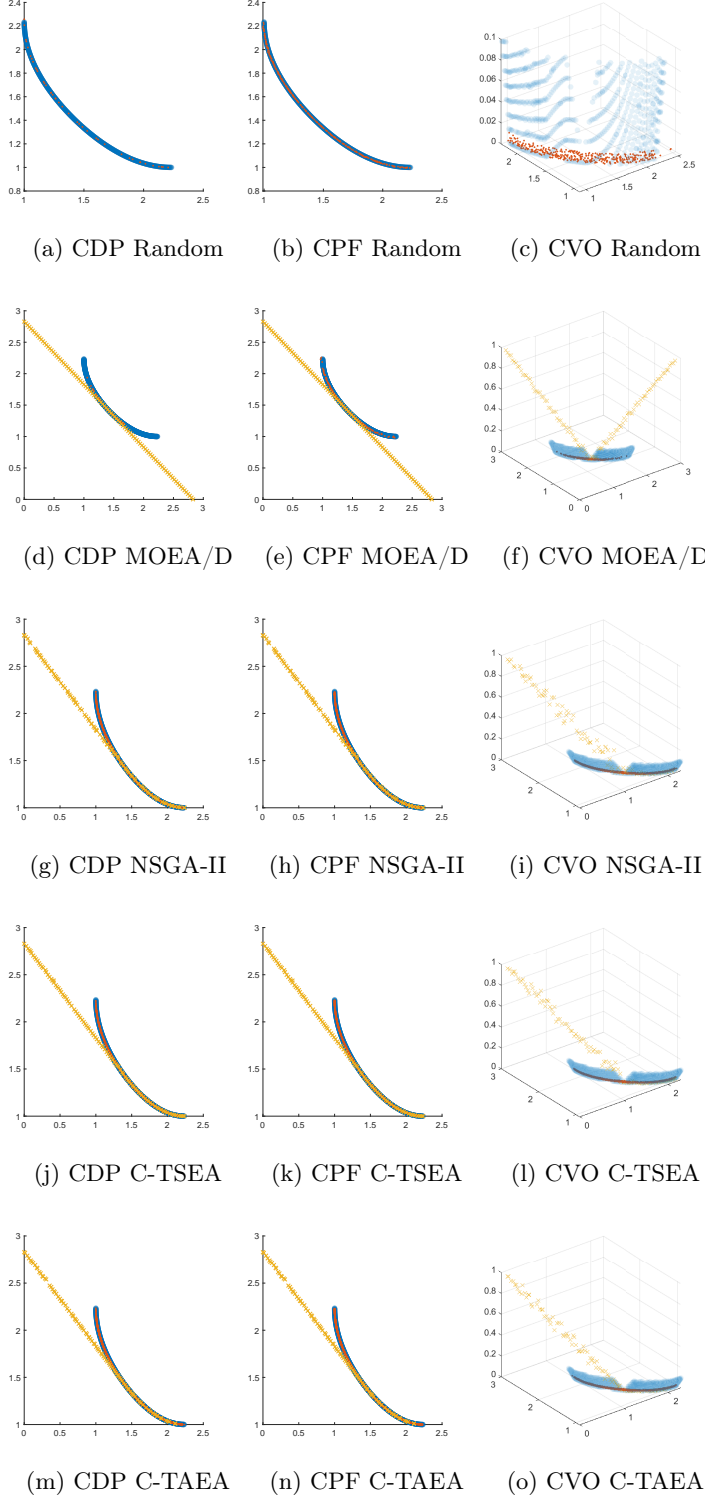


Fig. 12. Results obtained by the three archivers (represented by red dots) along with the final population of each MOEA (represented by yellow crosses) for the EqCo1 problem. The Pareto front is shown in blue.

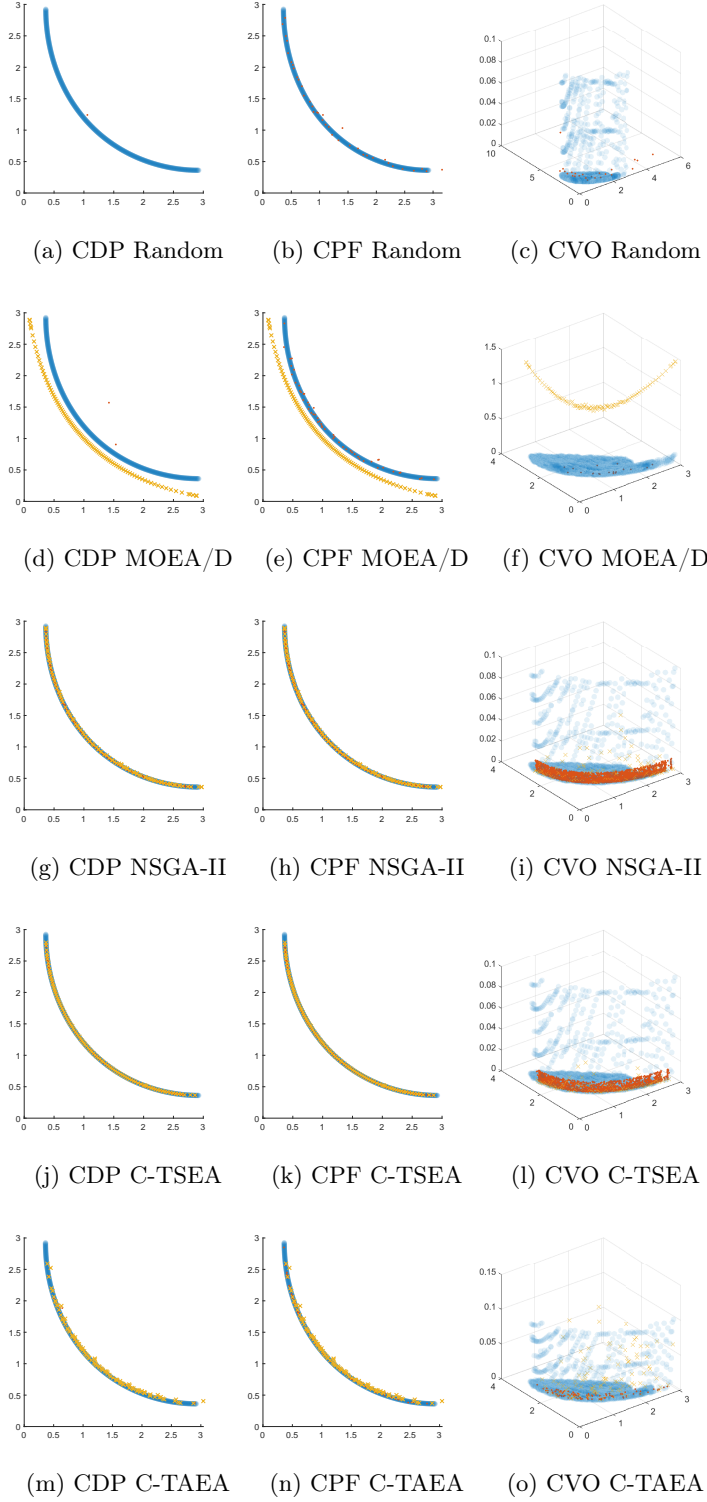


Fig. 13. Results obtained by the three archivers (represented by red dots) along with the final population of each MOEA (represented by yellow crosses) for the EqCo2 problem. The Pareto front is shown in blue.

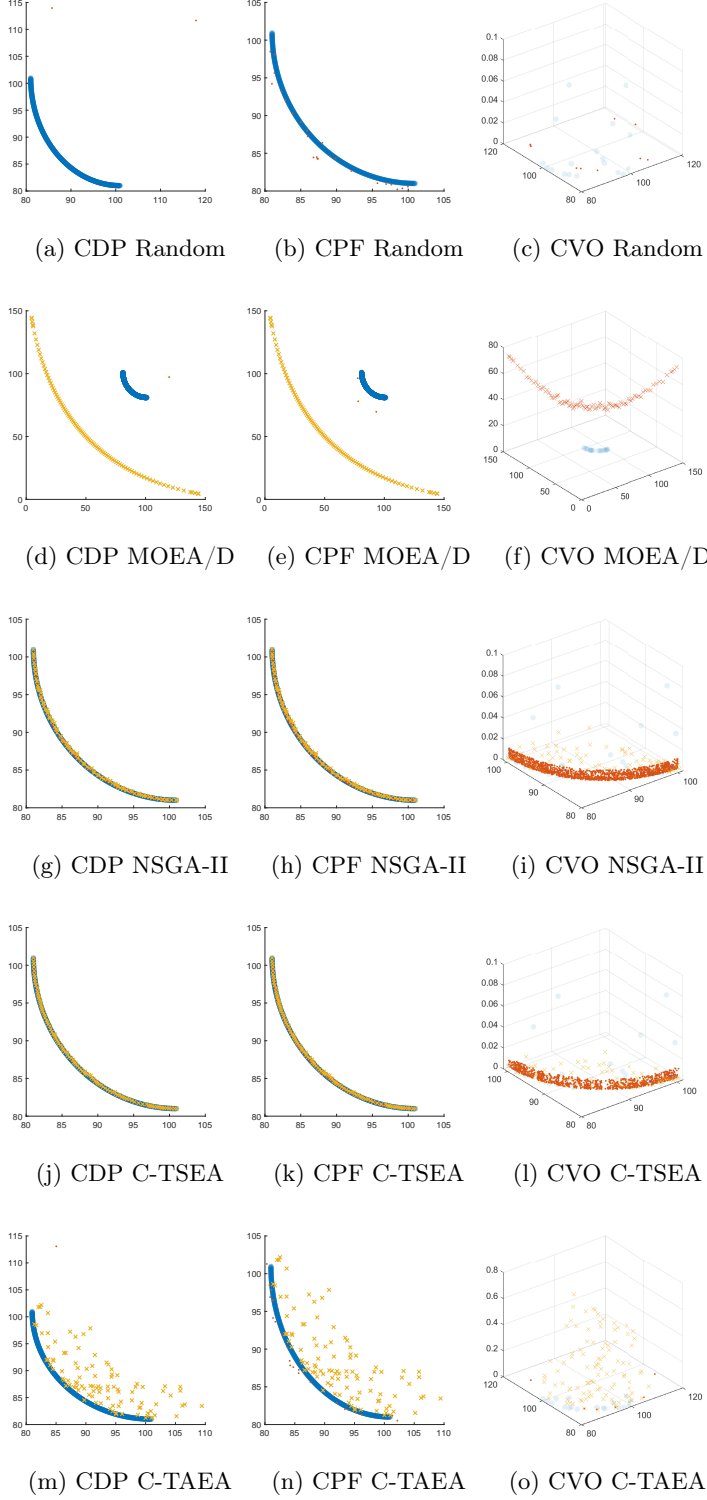


Fig. 14. Results obtained by the three archivers (represented by red dots) along with the final population of each MOEA (represented by yellow crosses) for the EqCo3 problem. The Pareto front is shown in blue.

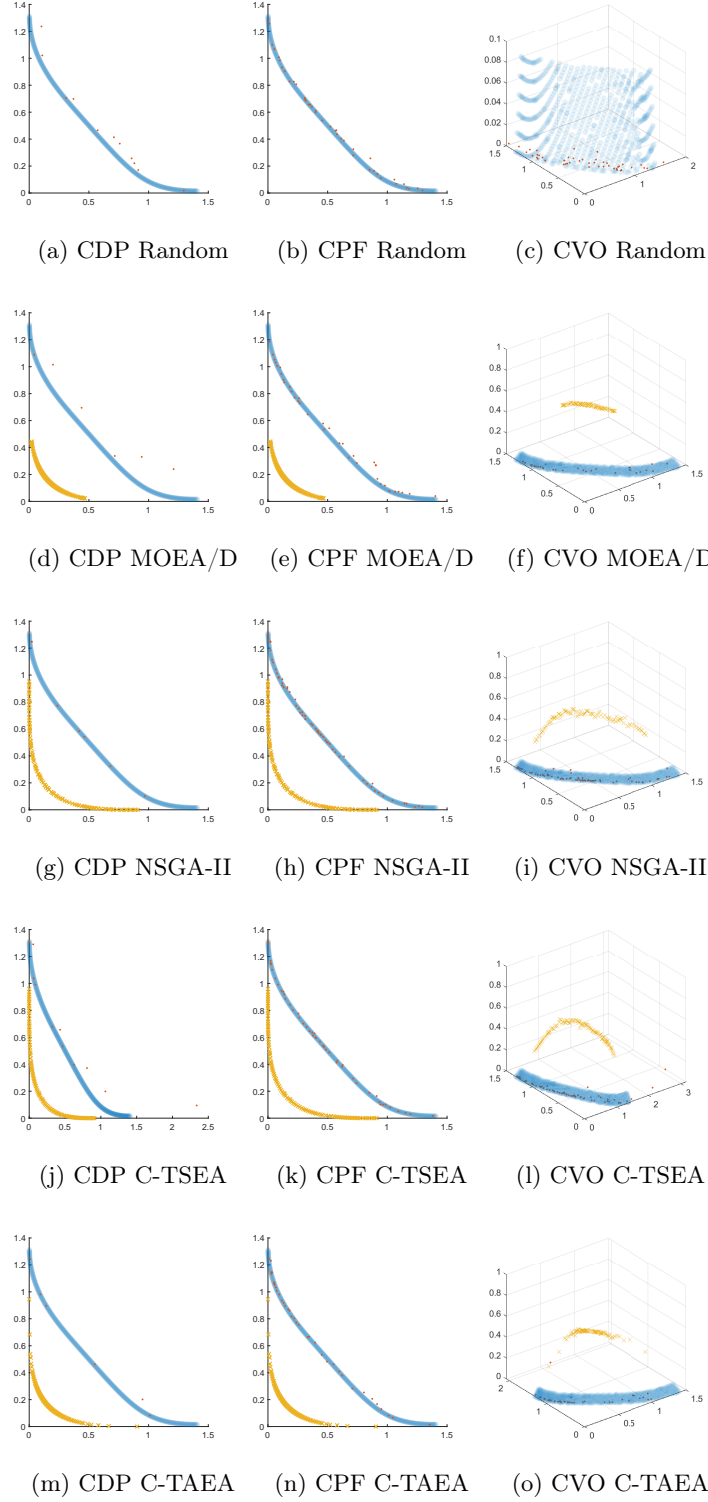


Fig. 15. Results obtained by the three archivers (represented by red dots) along with the final population of each MOEA (represented by yellow crosses) for the EqCo4 problem. The Pareto front is shown in blue.

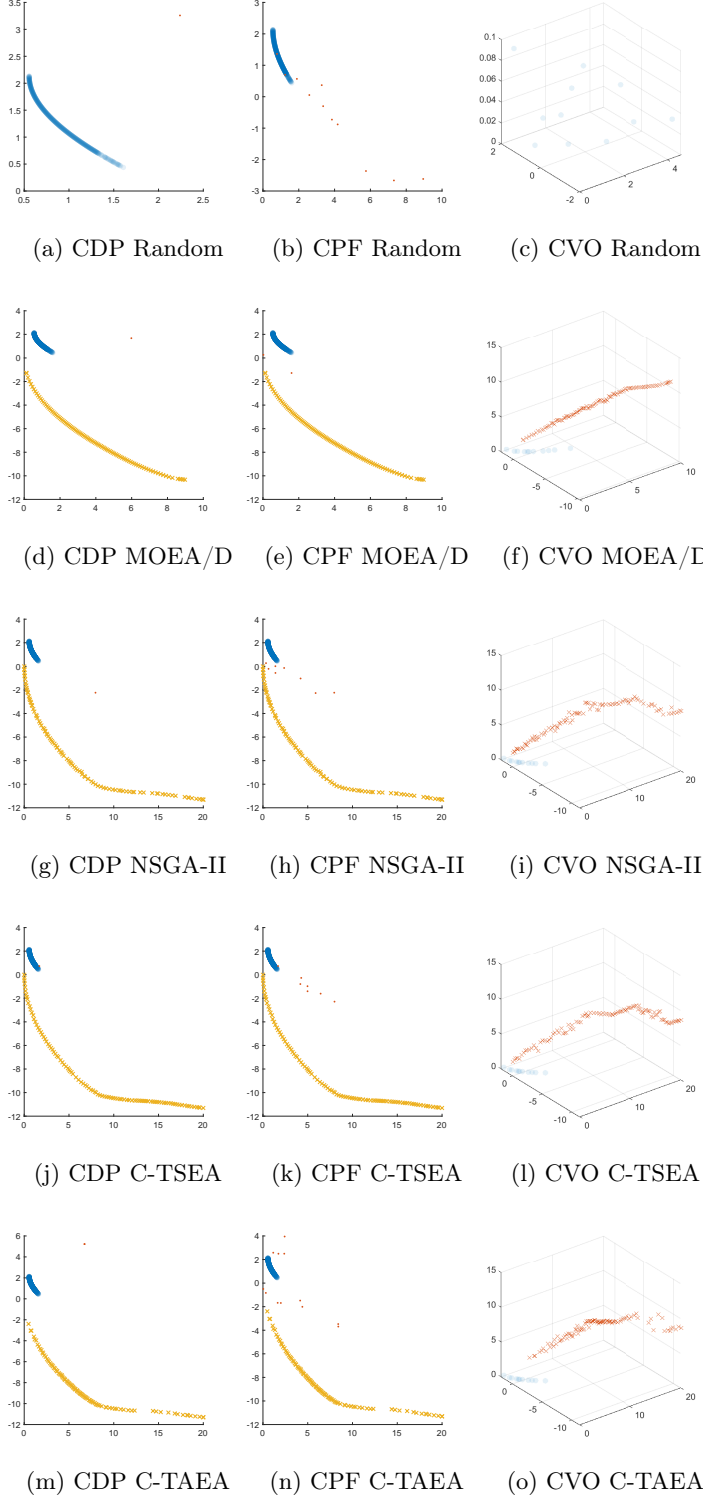


Fig. 16. Results obtained by the three archivers (represented by red dots) along with the final population of each MOEA (represented by yellow crosses) for the EqCo5 problem. The Pareto front is shown in blue.

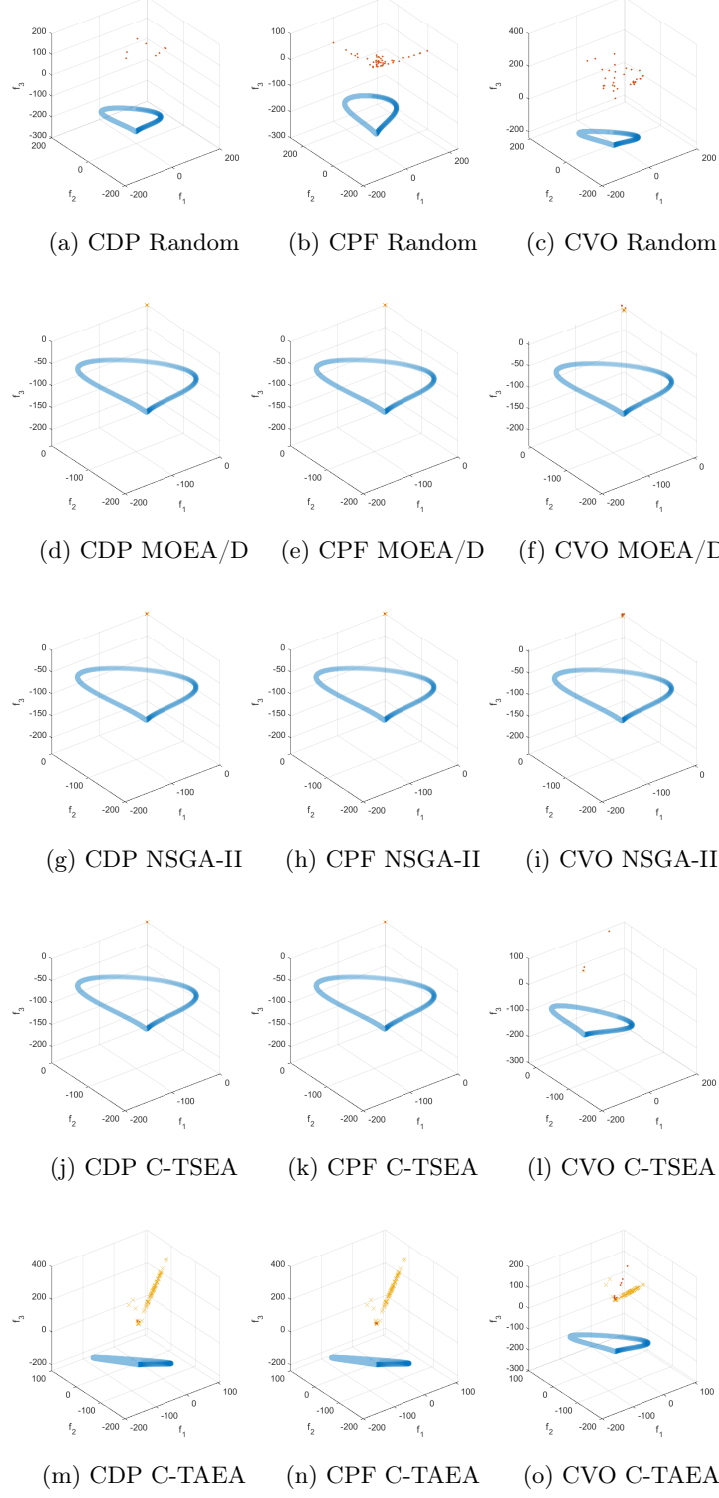


Fig. 17. Results obtained by the three archivers (represented by red dots) along with the final population of each MOEA (represented by yellow crosses) for the Eq1DTLZ1 problem. The Pareto front is shown in blue.

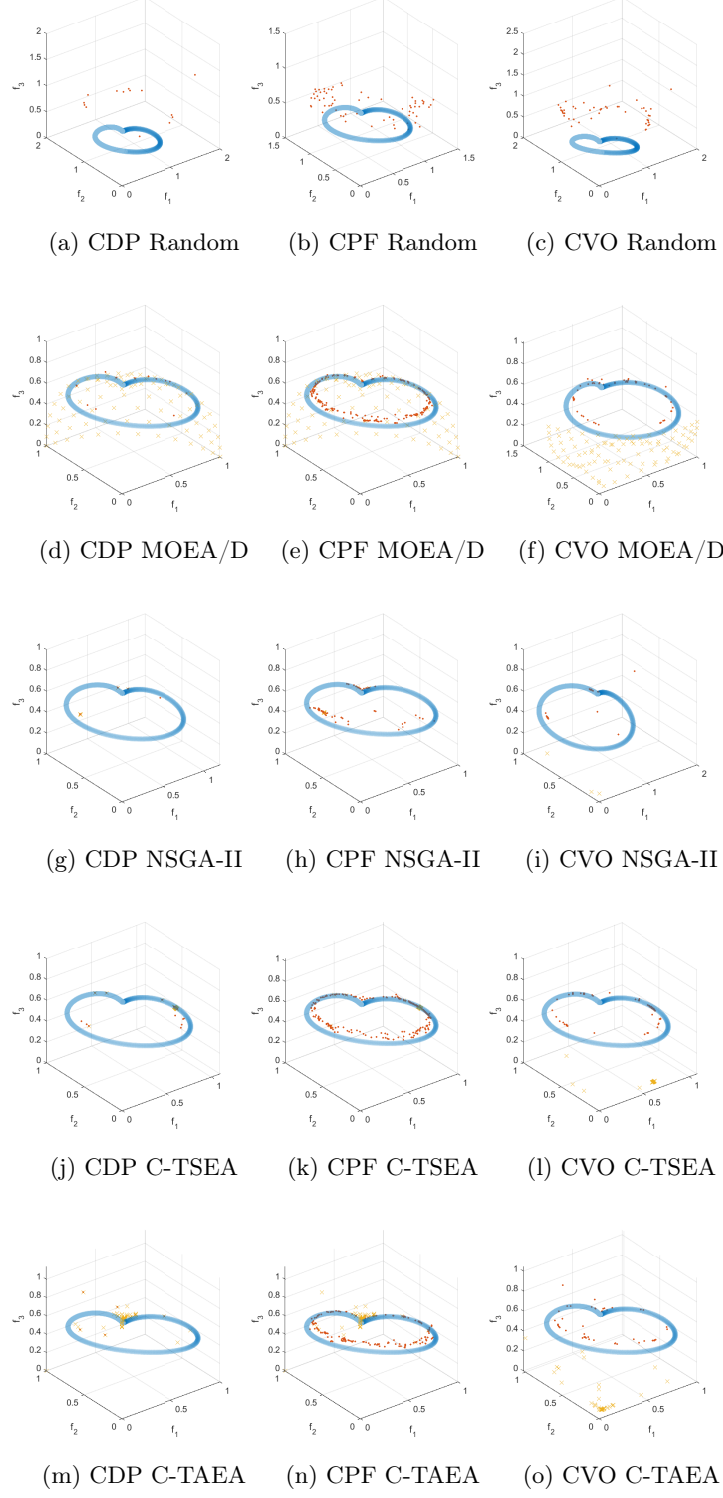


Fig. 18. Results obtained by the three archivers (represented by red dots) along with the final population of each MOEA (represented by yellow crosses) for the Eq1DTLZ2 problem. The Pareto front is shown in blue.

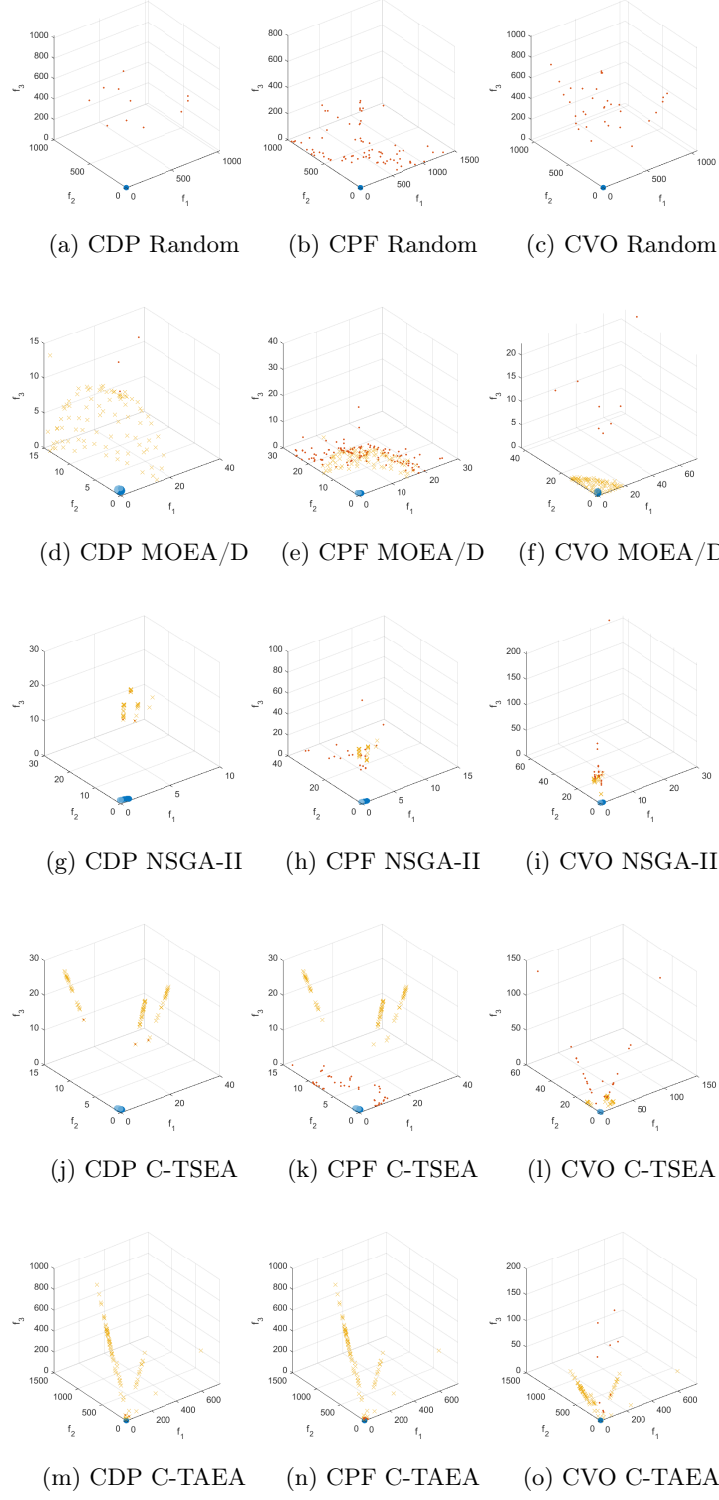


Fig. 19. Results obtained by the three archivers (represented by red dots) along with the final population of each MOEA (represented by yellow crosses) for the Eq1DTLZ3 problem. The Pareto front is shown in blue.

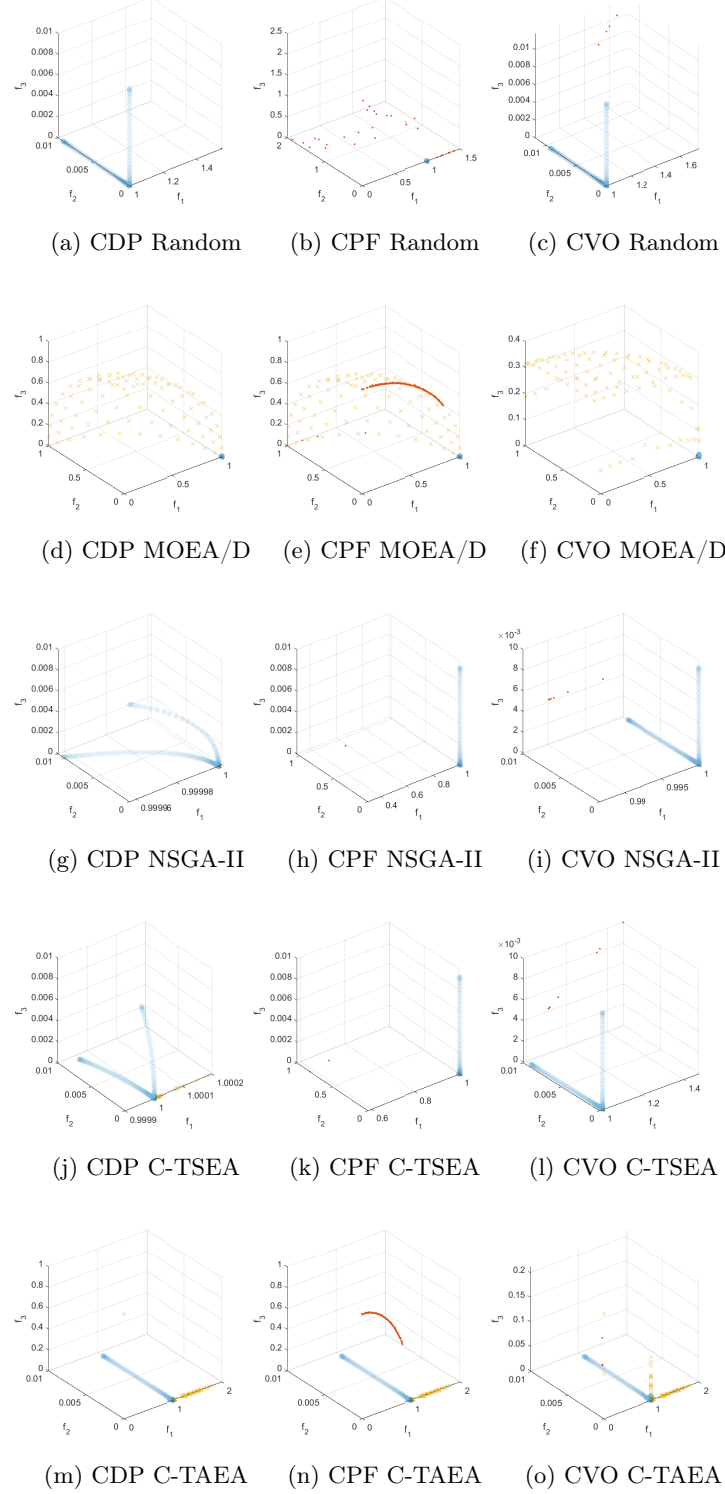


Fig. 20. Results obtained by the three archivers (represented by red dots) along with the final population of each MOEA (represented by yellow crosses) for the Eq1DTLZ4 problem. The Pareto front is shown in blue.

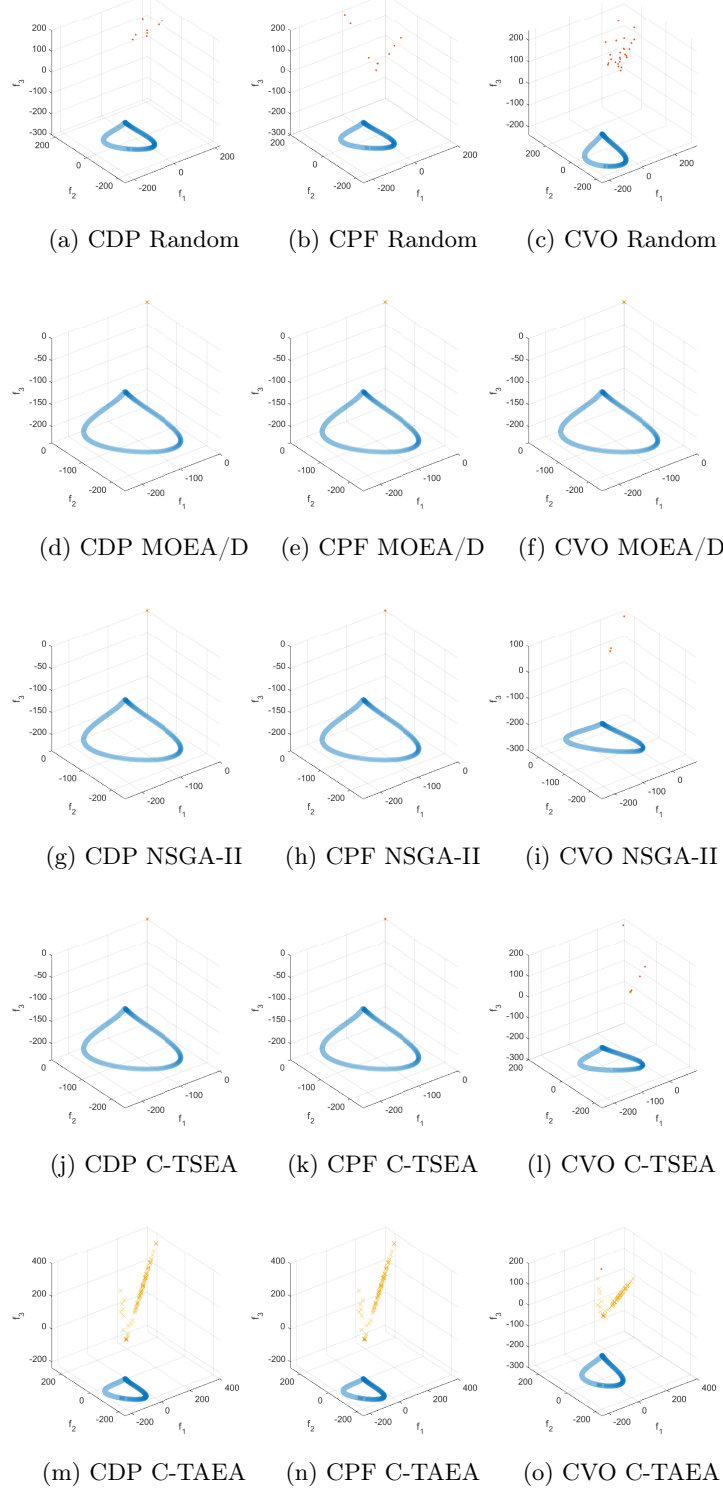


Fig. 21. Results obtained by the three archivers (represented by red dots) along with the final population of each MOEA (represented by yellow crosses) for the Eq1IDTLZ1 problem. The Pareto front is shown in blue.

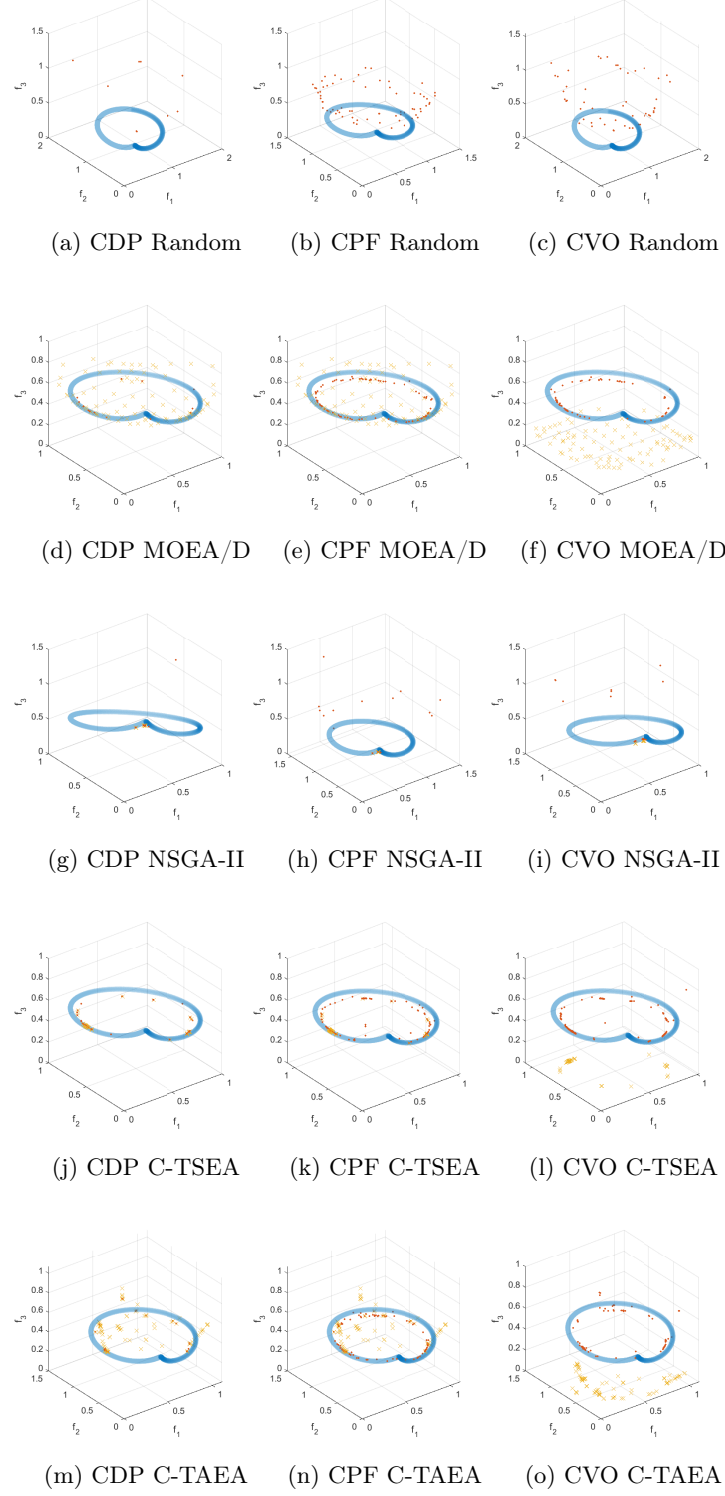


Fig. 22. Results obtained by the three archivers (represented by red dots) along with the final population of each MOEA (represented by yellow crosses) for the Eq1IDTLZ2 problem. The Pareto front is shown in blue.

4 Numerical Results of the CVO Approach with $\delta \rightarrow \infty$

A numerical analysis of CVO with $\delta \rightarrow \infty$ was performed for the EqCo benchmark. *ArchiveUpdateCVO* was fed with 1,000,000 points, and the results are shown in Figures 23-27. In those figures, the blue dots represent the Pareto set and front, the yellow dots show the results of the archive and the red dots indicate points with a $CV < 0.1$.

Simple functions such as EqCo1 show the expected result: the PS of MOP:CVO is a simple extension of the constrained PS (Figure 23). For EqCo2, where the constrained PS is an arc on the unit sphere, the PS for MOP:CVO is extended continuously. However, we observe that some additional solutions on the sphere are almost feasible (Figure 24). EqCo3 exhibits similar behaviour as EqCo1: the PS of MOP:CVO is a continuous extension of the constrained PS (Figure 25). EqCo4, however, show an interesting result. The constrained PS for this problem is a geodesic on the unit sphere, and the PS for MOP:CVO extends this geodesic into the interior of the sphere as seen in Figure 26. For EqCo5, Figure 27 shows the x_1, x_2, x_3 projection of the five decision variables, where the constrained PS is a curve that suddenly terminates. This may explain why several MOEAs have difficulty finding feasible points for this problem.

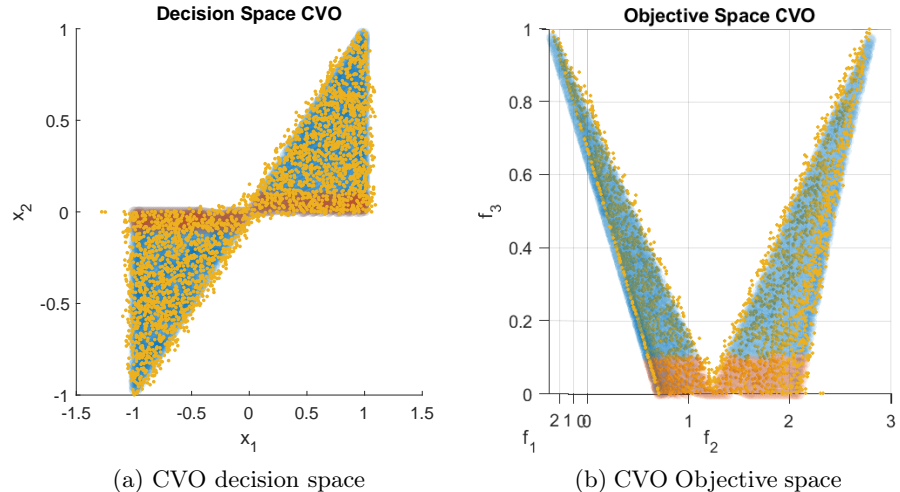


Fig. 23. Final result of the CVO approach for the EqCo1 problem. The Pareto set and front of MOP:CVO are shown in blue, along with the resulting archive in yellow. Points with a $CV < 10^{-2}$, representing an approximation of the PS for the unconstrained problem, are shown in red.

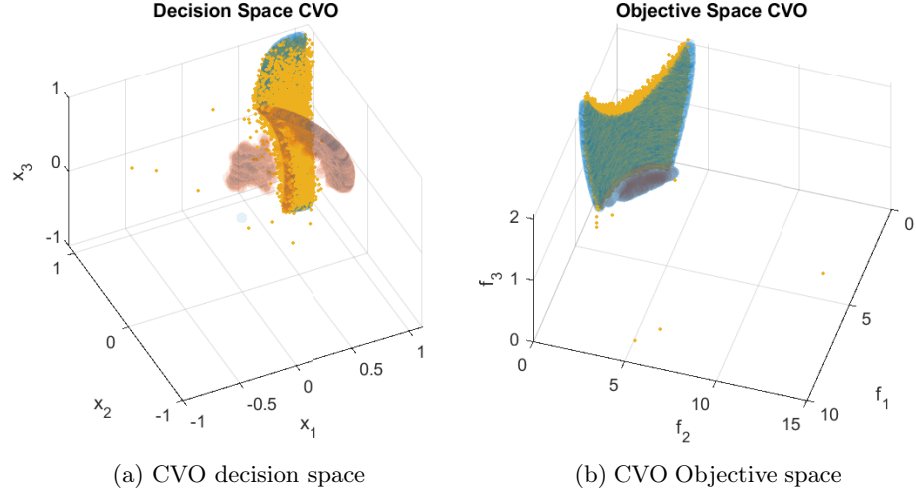


Fig. 24. Final result of the CVO approach for the EqCo2 problem. The Pareto set and front of MOP:CVO are shown in blue, along with the resulting archive in yellow. Points with a CV less than 10^{-2} , representing an approximation of the PS for the unconstrained problem, are shown in red.

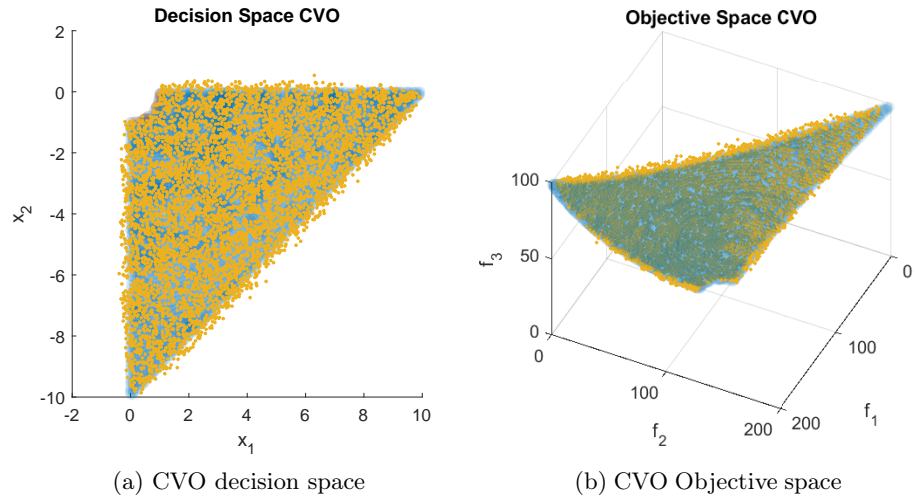


Fig. 25. Final result of the CVO approach for the EqCo3 problem. The Pareto set and front of MOP:CVO are shown in blue, along with the resulting archive in yellow. Points with a CV less than 10^{-2} , representing an approximation of the PS for the unconstrained problem, are shown in red.

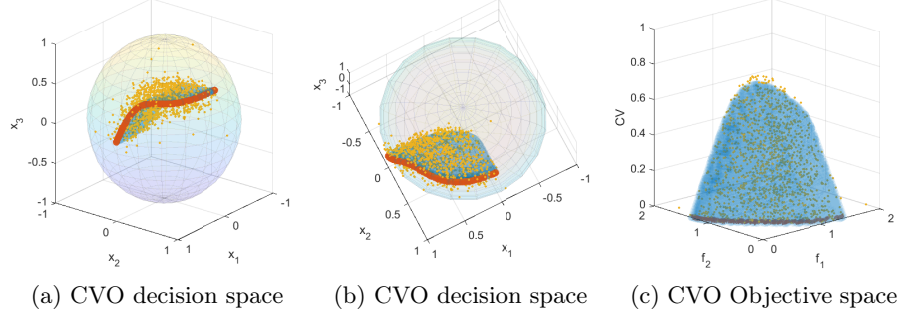


Fig. 26. Final result of the CVO approach for the EqCo4 problem. The Pareto set and front of MOP:CVO are shown in blue, along with the resulting archive in yellow. Points with a CV less than 10^{-2} , representing an approximation of the PS for the unconstrained problem, are shown in red. Figures (a) and (b) present two different angles of the decision space, while Figure (c) shows the objective space.

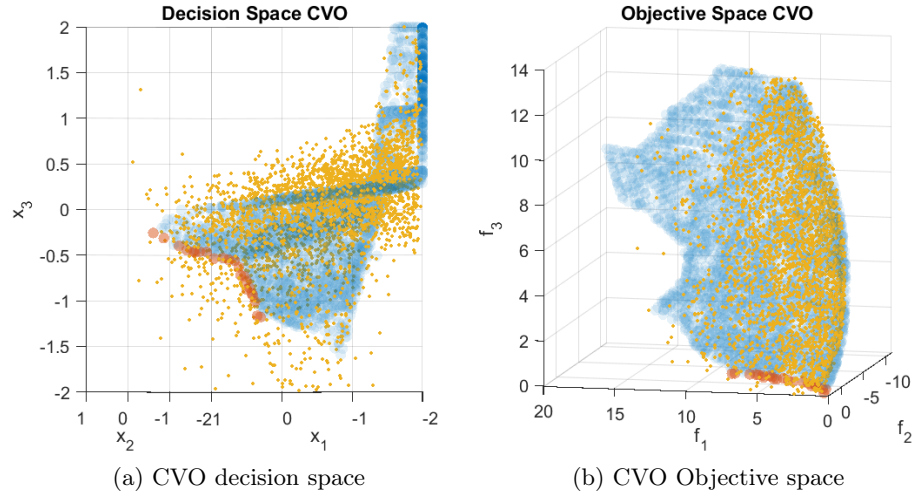


Fig. 27. Final result of the CVO approach for the EqCo5 problem. The Pareto set and front of MOP:CVO are shown in blue, along with the resulting archive in yellow. Points with a CV less than 10^{-2} , representing an approximation of the PS for the unconstrained problem, are shown in red.

5 Numerical Analysis of a Problem with an Empty Pareto Set

Additionally, a test function termed *emptytys* (6) was designed with an empty Pareto set to examine the outcomes in this scenario. For this function, the three archivers were fed with 1,000,000 random points, and we set the tolerance $\delta \rightarrow \infty$ for the CVO approach. The CDP approach found no solutions. The PF and the CDP approaches produced (infeasible) solutions: PF finds fewer solutions as μ increases (Figure 28), while CVO finds the best possible (infeasible) solutions, starting with a CV of 6 (Figure 29). Notably, even when the PS is empty, some approaches still identify backup (infeasible) solutions.

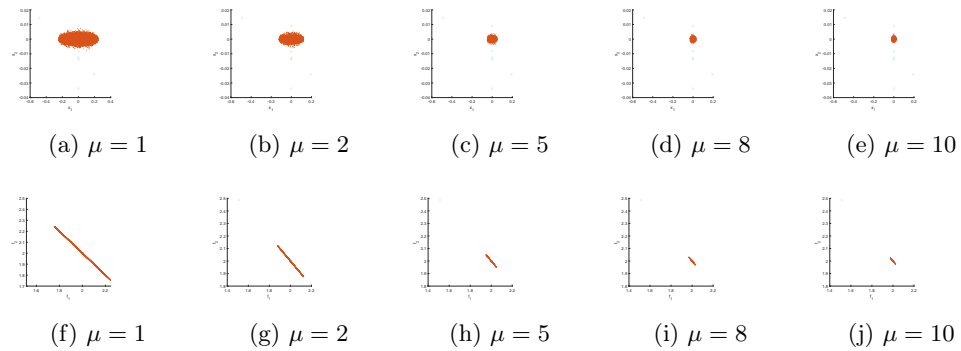


Fig. 28. Effect of μ for the problem *emptytys*.

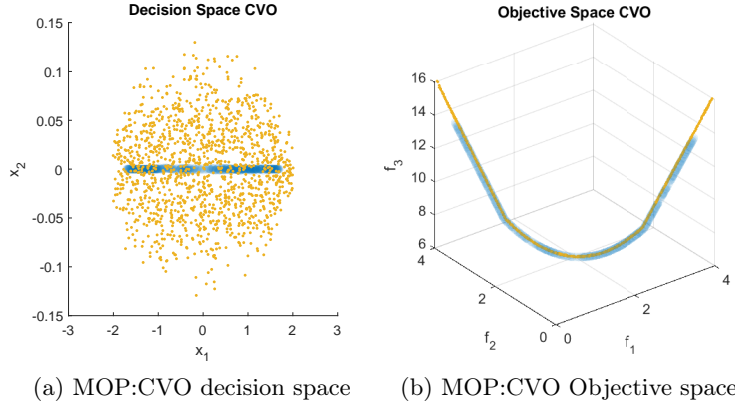


Fig. 29. Result of the CVO approach for the problem emptyps. The PS and PF for MOP:CVO are shown in blue, while the result of the random sampling is shown in yellow.

References

1. Martín, A., Schütze, O.: Pareto tracer: A predictor-corrector method for multi-objective optimization problems. *Engineering Optimization* **50**(3), 516–536 (2018)